

A decade of
Hubble Space Telescope
science

Proceedings of the
Space Telescope Science Institute Symposium,
held in Baltimore, Maryland
April 11–14, 2000

Edited by

MARIO LIVIO

Space Telescope Science Institute, Baltimore, MD 21218, USA

KEITH NOLL

Space Telescope Science Institute, Baltimore, MD 21218, USA

MASSIMO STIAVELLI

Space Telescope Science Institute, Baltimore, MD 21218, USA

Published for the Space Telescope Science Institute



CAMBRIDGE
UNIVERSITY PRESS

PUBLISHED BY THE PRESS SYNDICATE OF THE UNIVERSITY OF CAMBRIDGE
The Pitt Building, Trumpington Street, Cambridge, United Kingdom

CAMBRIDGE UNIVERSITY PRESS
The Edinburgh Building, Cambridge CB2 2RU, UK
40 West 20th Street, New York, NY 10011-4211, USA
10 Stamford Road, Oakleigh, VIC 3166, Australia
Ruiz de Alarcón 13, 28014 Madrid, Spain
Dock House, The Waterfront, Cape Town 8001, South Africa

<http://www.cambridge.org>

© Cambridge University Press 2003

This book is in copyright. Subject to statutory exception
and to the provisions of relevant collective licensing agreements,
no reproduction of any part may take place without
the written permission of Cambridge University Press.

First published 2003

Printed in the United Kingdom at the University Press, Cambridge

Typeface Computer Modern 10/12 pt. *System* L^AT_EX 2_ε [UPH]

A catalogue record of this book is available from the British Library

A catalogue record for this book is available from the British Library

Space Telescope Science Institute Symposium (2000 : Baltimore, Md.)

A decade of HST science : proceedings of the Space Telescope Science Institute
Symposium, held in Baltimore, Maryland, April 11-14, 2000/edited by Mario Livio,
Keith Noll, Massimo Stiavelli.

p. cm. (Space Telescope Science Institute symposium series; 14)

Includes bibliographical references and index.

ISBN 0 521 82459 1 (hardback)

1. Hubble Space Telescope (Spacecraft)—Congresses. I. Title. II. Series.

QB500.268.S6237 2000
520'.7'2—dc21 2002031076

Contents

<i>Participants</i>	vii
<i>Preface</i>	x
<i>HST</i> studies of Mars	
<i>J. F. Bell III</i>	1
<i>HST</i> images of Jupiter's UV aurora	
<i>J. T. Clarke</i>	25
Star formation	
<i>J. Bally</i>	44
SN1987A: The birth of a supernova remnant	
<i>R. McCray</i>	64
Globular clusters: The view from <i>HST</i>	
<i>W. E. Harris</i>	78
Ultraviolet absorption line studies of the Galactic interstellar medium with the Goddard High Resolution Spectrograph	
<i>B. D. Savage</i>	101
<i>HST</i> 's view of the center of the Milky Way galaxy	
<i>M. J. Rieke</i>	119
Stellar populations in dwarf galaxies: A review of the contribution of <i>HST</i> to our understanding of the nearby universe	
<i>E. Tolstoy</i>	128
The formation of star clusters	
<i>B. C. Whitmore</i>	153
Starburst galaxies observed with the <i>Hubble Space Telescope</i>	
<i>C. Leitherer</i>	179
Supermassive black holes	
<i>F. D. Macchetto</i>	198
The <i>HST</i> Key Project to measure the Hubble Constant	
<i>W. L. Freedman, R. C. Kennicutt, J. R. Mould, & B. F. Madore</i>	214
H_0 from Type Ia supernovae	
<i>G. A. Tammann, A. Sandage, & A. Saha</i>	222
Strong gravitational lensing: Cosmology from angles and redshifts	
<i>A. Tyson</i>	247

HST studies of Mars

By JAMES F. BELL III

Department of Astronomy, Cornell University, 402 Space Sciences Building, Ithaca, NY
14853-6801

HST observed Mars during all 5 oppositions between 1990 and 1999, providing unique new observations of the planet’s atmosphere and surface during seasons which are typically poorly-observed telescopically and in wavelength regions or at spatial scales that are not at all observed by spacecraft. *HST* observations also filled a crucial gap in synoptic observations of Mars prior to 1998, during a time when no spacecraft were observing the planet. *HST* data have provided important new insights and understanding of the Martian atmosphere, surface, and satellites, and they continue to fulfill important spacecraft mission support functions, including atmospheric aerosol characterization, dust storm monitoring, and instrument cross-calibration.

1. Introduction

Mars has been the subject of intense telescopic observations for centuries (see, for example, reviews by Martin et al. 1992 and Sheehan 1988). Interest in the red planet stems partly from its prominent appearance in the night sky as a bright extended object roughly every 26 months, and also from historic telescopic observations and more recent spacecraft encounters that have revealed many similarities between Mars and the Earth in terms of surface and atmospheric characteristics and climatic histories. While cold and arid today and probably inhospitable to most forms of life, evidence exists indicating that Mars once may have had a much more clement climate, during a postulated “warm and wet” epoch early in solar system history (e.g. Pollack et al. 1987; Carr, 1998).

The postulated similarities between early Mars and early Earth has fueled intense speculation and scientific interest on the question of life: could Mars have been (or still be?) a habitable environment for life to form, exist, and evolve? To answer this and other related questions requires a detailed understanding of both the past and present environment of Mars. While important clues have been provided by more than three decades of spacecraft flybys, orbiters, and landed investigations, these have been sporadic (and expensive!) glimpses of a complex planet, usually sampling only one part of the Martian seasonal cycle or one particular landing site in detail. For example, while the Viking Orbiter and Lander missions successfully observed the planet for more than two Mars years from orbit and from two widely-separated landing sites during the mid- to late-1970s, only one spacecraft successfully arrived at Mars during the 1980s (the Soviet Phobos-2 orbiter, which only operated for a few months), and the next successful missions after that didn’t occur until Mars Pathfinder, which landed in 1997, and the Mars Global Surveyor orbiter, which began mapping observations in 1997–98. Even these most recent missions were rather narrowly focused (Pathfinder on the local geology of a particular region; Global Surveyor on systematic high-resolution observations from a 2:00 a.m./2:00 p.m. Sun-synchronous orbit). Sadly, we have all been poignantly reminded of the inherent risks associated with spacecraft exploration of Mars recently, with the loss of both missions sent to Mars in 1999.

So, despite the incredible successes of many of the space missions sent to Mars, there is still clearly a niche for systematic synoptic-scale telescopic observations of the planet. Filling this niche requires several key instrumental characteristics, including: (a) high spatial resolution (less than hundreds of km), to resolve small-scale features on the surface and

in the atmosphere; (b) high data fidelity and accurate calibration, to detect weak photometric and/or colorimetric differences on the surface and in the atmosphere; and (c) good temporal sampling, in order to be able to quantify surface and atmospheric changes with season in the current Martian climatic regime. While meeting requirement (c) is possible from many large groundbased telescopes, meeting both requirements (a) and (b) in addition is usually not possible from groundbased platforms. This is because the Earth's atmosphere blurs resolution out to a large fraction of an arcsec even during the best seeing conditions (translating to more than several hundred km on Mars even at an excellent Mars opposition), and telluric water vapor and other species produce time-variable absorption features at key wavelengths that could otherwise be use to detect atmospheric and surface constituents on Mars. Rarely, when requirement (a) or (b) has been met by groundbased observations, the data have revealed that it is possible to detect and quantify variations in surface and atmospheric materials (e.g. Singer et al. 1979; Bell et al. 1990; Merényi et al. 1988; Bell and Crisp, 1993).

HST provides the ability to meet all of the requirements for scientifically-meaningful observations of Mars that complement, rather than duplicate, existing or ongoing spacecraft observational programs. Maximizing the ability of *HST* observations to advance Mars science has been a primary goal of all the observations conducted between *HST* Cycles 0 and 9. In this paper I will describe some of the outstanding unresolved issues in Mars studies, and describe the rationale and justification for the use of *HST* to observe such a close and bright object ($z \ll 1$). Next I will describe the observations of Mars that have been obtained by *HST* between 1990 and 1999. The results and scientific implications of the data will be discussed, broken down into the categories of Martian atmosphere, Martian surface, and Martian satellites. Special attention will be paid to describing how these *HST* measurements have played a role in shaping the acquisition and interpretation of ongoing or planned Mars orbital and landed spacecraft datasets. Finally, I will discuss future opportunities for Mars observations with *HST*, and how new data could continue to expand our understanding of the planet.

2. Outstanding issues in Mars studies

Mars is an enigmatic and fascinating planet. It is the most “Earth-like” of the other planets in the solar system. Evidence from decades of telescopic and spacecraft observations reveal geologic and isotopic evidence for substantial changes in the Martian climate during the early history of the planet. Specifically, degraded/eroded landforms, the presence of dendritic valley networks, and isotopic fractionation indicative of the loss of what was once a more substantial atmospheric indicate that the planet may have experienced a “warm and wet” climate regime (Pollack et al. 1987; Carr, 1999) with temperatures substantially above the melting point of water during the first billion years of its evolution. It is unknown whether this clement period in Martian history was short- or long-lived, though, or whether there were multiple such periods in response to planetary orbital/inclination variations or other external forcing processes. The duration and extent of stable liquid water at or near the Martian surface has important and different implications for the geologic and possibly biologic evolution of Mars, and understanding the history and role of water and its implications for climate and life are now the major drivers in NASA's Mars exploration program. Recent announcements concerning the possible presence of fossilized life forms in a Martian meteorite (McKay et al. 1996) and the possible presence of liquid water very close to the Martian surface (Malin & Edgett 2000), while controversial, underscore the intense public and scientific interest in Mars and the role that Martian studies play in larger exobiologic debates.

But understanding of the past climate conditions on Mars cannot be achieved without first understanding the present climate. Mars today is a cold and arid world with a thin atmosphere (tens of mbar) and (probably) little or no internal geologic activity. Conditions at the surface are influenced by seasonal and interannual cycles of CO₂ condensation and sublimation at the poles, by the exchange of small amounts of water vapor (tens of μm) between the atmosphere and the regolith, and by the radiative and physical influence of local- and global-scale atmospheric dust (James et al. 1992). The water, CO₂, and dust cycles have been studied intensely by spacecraft, but only at infrequent intervals or for relatively short periods of time. The historic telescopic record reveals that Mars has a dynamic and changing atmosphere and surface on timescales of decades to even centuries (Martin et al. 1992; McKim et al. 1999), and so understanding of the character of these cycles and of the planet's surface-atmosphere interactions must be teased out of both high-resolution focused measurements and long-timescale synoptic observations.

Some specific issues that remain elusive in our understanding of the current Martian atmosphere include: (1) What is the composition, distribution, and opacity of atmospheric aerosols (silicate dust, water ice, CO₂ ice, other aerosols?) and how does that composition change in response to diurnal and seasonal timescale variations in radiative forcing? (2) What is the radiative influence of airborne dust and/or clouds on the energy balance of the Martian atmosphere, and how do these aerosols tangibly influence the climate (temperature, pressure changes due to volatile condensation, local winds). (3) What are the dominant styles and rates of dust and volatile transport in the Martian atmosphere, and how are they influenced by topography, albedo, and seasonal climate variations? And (4) What is the magnitude of the present variability of the Martian climate (seasonal temperature and pressure extrema, dust storm frequency, atmospheric opacity) on yearly, interannual, and even longer timescales decipherable from the telescopic and geologic record?

Understanding the nature of the present Martian surface also plays a key role in determining the climatic and geologic history of the planet. Surface geologic activity like volcanism, tectonism, and impact processes are obvious manifestations of the geologic evolution of the planet. In some cases, these processes can have important effects on the climate, such as the release of greenhouse gases by volcanic eruptions and the heat flux created during large impact cratering events. Most of our understanding of the detailed surface geology of Mars has come from orbital and landed spacecraft observations during the past few decades. These observations have shown that at increasing spatial resolutions, the detailed geomorphology of Mars looks less and less like that of the Earth (e.g. Malin et al. 1998), reflecting instead the specific style and nature of uniquely Martian geologic processes. This underscores an important point: Mars is truly a different world than the Earth, and while the planet's surface and atmospheric processes are dictated by the same physics and chemistry driving familiar processes here, the timescales and boundary conditions for geologic and climatic activity on Mars are substantially different from those on the Earth.

Some of the specific issues that remain outstanding in our study of the Martian surface include: (1) What is the composition and mineralogy of the surface rocks and soils and the airborne dust, and what do the chemistry and mineralogy reveal about the current and (especially) past Martian climate? On Earth, many kinds of rocks and minerals preserve a record of local climate conditions during their formation. Examples include hydroxides, carbonates, and sulfates, which can sequester atmospheric gases into their crystalline structures; and Fe(III) oxides, which have polymorphs that form within specific temperature, pH, humidity, and $f(\text{O}_2)$ conditions. Some of these minerals are stable

or metastable under current Martian climatic conditions but not in a perhaps warmer, wetter past, meaning that their detection and characterization could also provide information on the extent and timing of climate change over the course of the planet's history. (2) What are the sources and sinks of volatiles (especially water) and the nature and rate of surface/atmosphere volatile exchange on Mars? This is a key question in Martian climate studies, as noted above, and includes not only the mineralogy issues just discussed, but also the growth and decay of the planet's seasonal H₂O and CO₂ polar ice caps, the diurnal exchange of water vapor between the surface and atmosphere, and the controversial issue of deep or shallow subsurface liquid water on Mars, and its possible role in alteration of surface materials and formation of localized geologic features (e.g. Malin & Edgett 2000). And (3) What are the dominant processes responsible for changing the albedo and overall geology of the surface with time? These include aeolian processes like dust storms on a variety of scales and which have been recorded telescopically for centuries, as well as volcanic, tectonic, and impact processes that modify the surface on much longer timescales but whose effects are preserved in the current topography and landforms of the planet.

3. Why Use *HST*?

But why use *HST* to observe Mars, given the fierce competition for *HST* observing time, the availability of large groundbased telescopes to observe the planet, and, more importantly, the armada of spacecraft that have studied the planet or will visit in the near future? There are five primary reasons:

(a) *Spectral coverage in the ultraviolet.* UV astronomical observations in general provide an important component of *HST*'s mission in general because of the inability to observe from the ground at these wavelengths. For Mars, UV observations uniquely enable observations of atmospheric O₃. Ozone, though a trace component of the atmosphere (0.04 to 0.2 ppm), plays a critical role in Martian atmospheric photochemistry and also serves as a tracer of atmospheric water vapor transport. UV measurements also provide diagnostic information on atmospheric aerosols, including the ability to discriminate between H₂O and dust clouds as sources of atmospheric opacity. Finally, a number of iron-bearing mineral species have solid state absorption features at UV wavelengths due to Fe(II) and Fe(III) electronic transitions and Fe–O charge transfer transitions that vary systematically with crystalline structure, providing a way to identify the surface mineralogy from remote spectroscopic observations.

(b) *Spectral coverage outside of the Earth's atmospheric "windows."* Extinction caused by water, CO₂, O₂, and other gases and aerosols in the Earth's atmosphere prevents groundbased observations at wavelengths that provide unique information about the Martian surface and atmosphere. These include regions near 1 μm and 2 μm where characterization of subtle shifts in the widths and positions of broad iron-bearing silicate absorption features are hampered by telluric water; narrow and weak Martian water vapor bands that are completely obscured by their stronger telluric counterparts and which can only be observed when Doppler-shifted away from the telluric lines (and thus when the planet has a small apparent angular diameter from Earth); the wings of strong CO₂ bands, which provide information on the Martian atmospheric pressure and temperature profile but which are masked by comparably-strong telluric CO₂ lines, and parts of the near-infrared where both strong and weak bands caused by metal–OH absorptions and structural (bound) H₂O in minerals are masked by Earth's water, CO, and CO₂ bands.

(c) *Spatial resolution.* The near diffraction-limited performance of the corrected *HST* optics provides the ability to discern subtle spatial structures on the Martian surface

and atmosphere that are undetectable from the ground. Typical groundbased resolution on Mars is 150–300 km during good seeing conditions ($0''.5$) and during the month or so around opposition. Adaptive optics or speckle imaging techniques can be used to improve the groundbased resolution, but many of these techniques break down because Mars is so bright ($M_v \sim 4.5/\text{arcsec}^2$) and none have been shown to yield reliable spectrophotometric measurements of extended sources. WFPC2 on *HST* allows resolutions as fine as ~ 20 km/pixel around opposition, and ~ 50 km/pixel routinely for the \sim half of the Martian year observable within *HST* sun avoidance constraints. These kinds of resolutions are comparable to those obtained by the Mariner flyby spacecraft in the late 1960s, the Viking orbiter global approach observations in the mid-1970s, the Phobos-2 imaging spectroscopy measurements of the late 1980s, and are within a factor of ~ 3 of the Mars Global Surveyor (MGS) Thermal Emission Spectrometer (TES) measurements that are currently being obtained.

(*d*) *Mission Support*. In a sense, *HST* is another NASA “mission” to Mars, providing the ability to obtain both synoptic-scale imaging and spectroscopy and fine-spatial regional investigations of the surface and atmosphere. *HST* measurements fill a crucial gap in spacecraft coverage. Because of the loss of the Mars Observer spacecraft in 1993, between the Phobos-2 mission in 1989 and the MGS mission in 1998 there were no spacecraft observations of Mars. The importance and need for high quality supporting telescopic observations of Mars even in an era of expanded planetary missions was reinforced during 1999 with the failure of both the Mars Climate Orbiter (MCO) and Mars Polar Lander missions. MCO in particular would have provided substantial new multispectral and atmospheric sounding data highly complementary to the types of measurements being performed by *HST*. In the absence of these orbital or landed missions, *HST* has continued to provide both the best monitoring observations and the only new measurements of Mars surface and atmospheric phenomena. The planetary science community has embraced this role for the telescope, and fully expect *HST*’s contributions to continue to include important and unique NASA spacecraft mission support functions as well as new science results.

(*e*) *Public relations and outreach*. *HST*’s images of Mars are spectacular, and they fulfill important non-scientific NASA goals by providing inspirational and educational information about an object that is both familiar and interesting to the general public. Mars has long fascinated the public because of its Earthlike characteristics and the potential for past or even present life on its surface. Scientists and educators capitalize on this nascent interest and have used *HST* and other mission’s images and information about Mars to teach concepts of astronomy, geology atmospheric science, celestial mechanics, and even biology. The education and outreach impact can be assessed by the many K–12 curriculum materials, museum exhibits, ST ScI press releases (11), and general interest newspaper and magazine articles that have been produced based on *HST* Mars images and other data.

4. Observations

Earth to Mars oppositions occur every ~ 26 months, with Mars closest approach distance varying from 56 to 101 million km over a ~ 15 year period because of the eccentricity of the Martian orbit. The inclination of Mars (25°) is similar to the Earth’s, and the planets’ orbital cycles are phased so that oppositions occur at successively advancing Martian seasons during the ~ 15 year cycle (Figure 1). Mars southern hemisphere summer occurs near the perihelion of its orbit and coincides with the closest Earth to Mars oppositions, providing the best possible spatial resolution. The worst oppositions

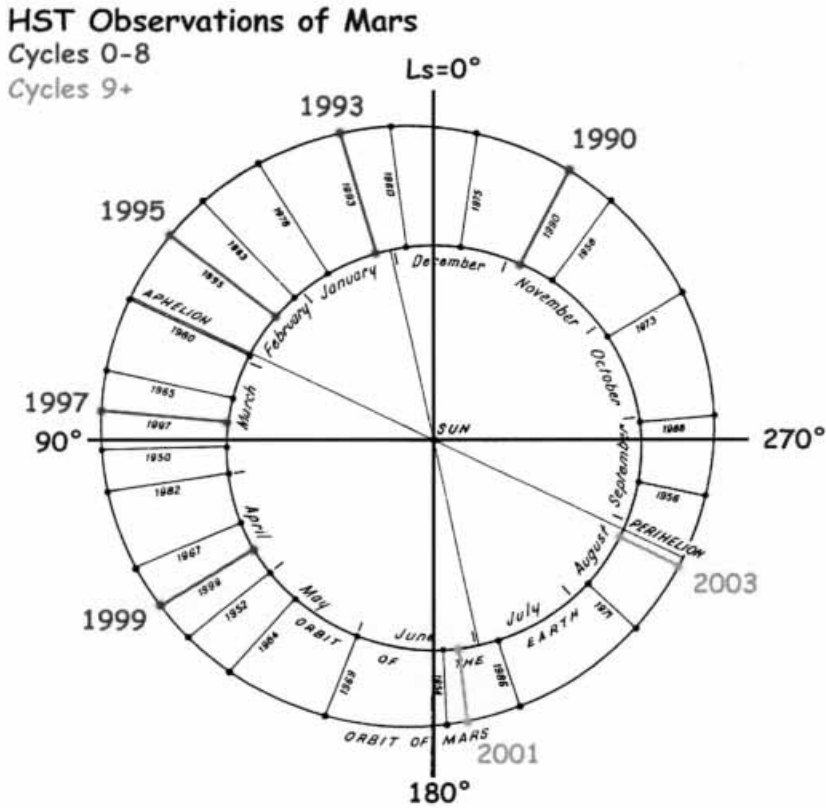


FIGURE 1.

in terms of spatial resolution occur near Martian aphelion, meaning that northern hemisphere summer is the least well studied period of the Martian year.

4.1. *Imaging*

Table 1 summarizes *HST* Imaging Observations during Cycles 0–8 (1990 to 1999). Early Cycle 0–3 WF/PC observations were limited in terms of resolution by the uncorrected spherical aberration of the *HST* primary. In addition, observing time was initially allocated in units of hours, allowing time for usually no more than 6–7 images per visit. As a result, the focus of imaging observations was on UV and blue exposures to study aerosols, and on a modest amount of red and green imaging in order to generate true color images of the planet. A small number of additional near-IR exposures was obtained to try to characterize the spectral behavior of the surface at longer wavelengths. Visit spacings were timed to try to sample the Martian seasonal cycle at intervals corresponding to the timescale of changes observed in the historic telescopic record (e.g. Martin et al. 1992). Occasional visits were conducted on the same Martian sol (a sol is one Martian “day.” or 24 hours 37 minutes) in order to search for diurnal variations as well as to construct global maps covering all longitudes.

UT Date ^a YYMMDD	Time, ^b UT	Wavelengths, nm	Diameter, arcsec	SE Lat, deg	SE Lon, deg	Phase, deg	L_s , deg	Resolution, ^c km/pixel	PROGID ^d
<i>HST Cycle 0 data: WF/PC</i>									
901213a	10:34	230, 336, 439, 502, 588, 673, 889	16.6	-11.8	184.8	13.4	348.6	~60°	3103, James
901213b	18:39	230, 336, 439, 502, 588, 673, 889	16.6	-11.8	303.1	13.6	348.8	~60	3103, James
901214	02:43	230, 336, 439, 502, 588, 673, 889	16.6	-11.9	61.1	13.9	348.9	~60	3103, James
<i>HST Cycle 1 data: WF/PC</i>									
910102	05:31	413, 502, 673	13.7	-13.1	290.7	25.9	358.7	~68	3107, James
910207	04:49	230, 336, 413, 673	9.4	-10.0	305.3	36.2	1.6	~100	3107, James
910320	06:43	413, 673	6.5	-1.8	302.8	37.3	35.3	~145	3107, James
910514	16:53	230, 336, 413, 502, 673	5.0	11.7	282.2	31.7	59.9	~188	3107, James
910515a	01:12	413, 673	5.0	11.7	43.6	31.6	60.0	~188	3107, James
910515b	09:15	413, 673	5.0	11.8	161.1	31.6	60.1	~188	3107, James
<i>HST Cycle 2 data: WF/PC</i>									
920530	03:40	413, 673	5.4	-22.6	300.4	34.5	259.0	~175	3763, James
920611	20:56	413, 673	5.4	-20.4	73.7	35.9	267.0	~175	3763, James
920627	22:57	336, 413, 673	5.8	-16.8	305.8	37.6	277.1	~162	3763, James
920709	15:13	413, 673	5.8	-13.9	75.4	38.7	284.3	~162	3763, James
921005	01:03	230, 336, 413, 502, 673	8.3	8.1	98.1	41.9	335.2	~114	3763, James
921101a	06:00	336, 413, 502, 588, 673, 889	10.1	11.9	274.5	38.5	349.5	~93	3763, James
921101b	15:13	336, 413, 502, 588, 673, 889	10.1	11.9	49.1	38.4	349.7	~93	3763, James
<i>HST Cycle 3 data: WF/PC</i>									
930102a	04:19	413, 502, 588, 673, 889, 1042	15.1	8.3	47.5	5.5	20.0	~62	4771, James
930102b	12:21	336, 413, 502, 588, 673, 889	15.1	8.2	165.1	5.3	20.1	~62	4771, James
930102c	20:32	413, 502, 588, 673, 889	15.1	8.1	284.9	5.0	20.3	~62	4771, James
930409	16:27	413, 502, 673	7.2	10.4	59.0	37.0	63.8	~131	3763, James
930411	06:43	336, 413, 502, 673	7.2	10.7	257.8	37.0	64.5	~131	3763, James
930616	15:13	413, 502, 673	5.0	22.5	106.7	32.4	93.6	~189	3763, James

TABLE 1. HST WF/PC, WFPC2, and NICMOS observations of Mars: 1990–1999

UT Date ^a YYMMDD	Time, ^b UT	Wavelengths, nm	Diameter, arcsec	SE Lat, deg	SE Lon, deg	Phase, deg	L_s , deg	Resolution, ^c km/pixel	PROGID ^d
<i>HST Cycle 4 data: WFPC2</i>									
940806	07:52	547	5.0	0.1	231.0	32.1	326.0	61.5 ^f	5493, James
940823	23:00	255, 336, 410,502, 673	5.2	5.1	287	34.4	335.7	59.1	5493, James
940919	15:15	255, 336, 410,502, 673	5.7	11.8	273	36.5	349.7	54.0	5493, James
941020	11:43	255, 336, 410,502, 673	6.5	17.7	282	38.3	5.3	46.8	5493, James
941118	05:35	255, 336, 410,502, 673	7.8	21.0	275	38.0	19.1	39.3	5493, James
950102	09:56	255, 336, 410,502, 673	11.2	21.8	278	28.0	39.7	27.3	5493, James
950223	13:26	255, 336, LRFs (bad), 1042	13.5	17.6	231	9.7	62.9	22.6	5215, Crisp
950224	17:00	255, 336, 410,502, 673	13.5	17.3	274	10.0	63.1	22.7	5493, James
950225a	01:00	255, 336, 410,502, 673	13.5	17.2	31	10.3	63.6	22.7	5493, James
950225b	09:00	255, 336, 410,502, 673	13.4	17.2	148	10.5	63.7	22.7	5493, James
950225c	20:07	255, 336, LRFs (bad), 1042	13.4	17.4	311	11.4	63.9	22.7	5215, Crisp
950226a	00:58	255, 336, LRFs (bad), 1042	13.4	17.4	22	11.6	64.0	22.7	5215, Crisp
950226b	05:52	255, 336, LRFs (bad), 1042	13.4	17.4	94	11.7	64.1	22.7	5215, Crisp
950408	19:22	255, 336, 410,502, 673	9.8	18.1	281	32.6	81.9	31.4	5493, James
950411	02:05	336	9.6	18.1	0	33.4	83.3	32.0	5215, Crisp
950528	01:46	255, 336, 410,502, 673	6.8	23.0	270	41.7	104.1	45.2	5493, James
<i>HST Cycle 5 data: WFPC2</i>									
950706a	03:20	255, 336, 410, 502, 673, 740, 860, 953, 1042	5.6	25.7	275	38.9	122.1	55.1	5832, James
950706b	11:23	255, 336, 410, 502, 673, 740, 860, 953, 1042	5.5	25.8	33	38.9	122.2	55.2	5832, James
950711	23:16	255, 336, 410, 502, 673, 740, 860, 953, 1042	5.4	25.8	157	38.1	124.8	54.0	5832, James
950802	21:21	255, 336, 410, 502, 673, 740, 860, 953, 1042	5.0	25.3	274	34.4	135.4	61.0	5832, James
950821	09:21	255, 336, 410, 502, 673, 740, 860, 953, 1042	4.8	23.5	273	30.8	144.6	64.4	5832, James

TABLE 1. *Continued*

UT Date ^a YYMMDD	Time, ^b UT	Wavelengths, nm	Diameter, arcsec	SE Lat, deg	SE Lon, deg	Phase, deg	L_s , deg	Resolution, ^c km/pixel	PROGID ^d
<i>HST Cycle 6 data: WFPC2</i>									
960918	20:01	218, 255, 336, 410, 502, 588, 673, 953, 1042	4.6	16.6	161	29.3	11.3	66.7	6741, James
961008	16:10	255, 336, 410, 502, 588, 673, 763, 835, 953, 1042	5.0	20.3	272	31.9	20.7	61.3	6741, James
961009	00:13	255, 336, 410, 502, 588, 673, 763, 835, 953, 1042	5.0	20.3	30	31.9	20.9	61.3	6741, James
961015	13:54	255, 336, 410, 502, 588, 673, 763, 835, 953, 1042	5.1	21.3	169	32.7	24.0	60.1	6741, James
961129	17:58	218, 255, 336, 410, 502, 588, 673, 953, 1042	6.4	24.5	154	36.3	44.5	47.9	6741, James
961230	05:48	218, 255, 336, 410, 502, 588, 673, 953, 1042	8.0	24.0	42	35.6	58.0	38.3	6741, James
970104a	00:15	218, 255, 336, 410, 502, 588, 673, 953, 1042	8.3	23.8	270	35.1	60.1	36.9	6741, James
970104b	17:41	218, 255, 336, 410, 502, 588, 673, 953, 1042	8.3	23.8	167	35.0	60.4	36.9	6741, James
970310a	06:28	255, 336, 433, 467, 554, 763, 835, 893, 953	14.0	22.8	135	6.2	88.6	21.9	6852, Crisp
970310b	11:18	255, 336, 433, 467, 554, 763, 835, 893, 953	14.0	22.8	204	6.1	88.7	21.9	6852, Crisp
970310c	17:46	255, 336, 433, 467, 554, 763, 835, 893, 953	14.0	22.8	299	5.9	88.8	21.9	6852, Crisp
970330a	04:03	255, 336, 410, 467, 502, 547, 588, 631, 673, 1042	14.0	23.4	284	10.7	97.4	21.9	6741, James
970330b	10:30	255, 336, 410, 467, 502, 547, 588, 631, 673, 1042	14.0	23.4	18	10.9	97.6	21.9	6741, James
970330c	12:07	255, 336, 433, 467, 554, 763, 835, 893, 953	14.0	23.4	42	11.0	97.6	21.9	6852, Crisp
970330d	15:21	255, 336, 410, 467, 502, 547, 588, 631, 673, 1042	14.0	23.4	90	11.1	97.7	21.9	6741, James
970330e	22:06	255, 336, 410, 502, 588, 673, 1042	14.0	23.4	288	11.3	97.8	21.9	6741, James
970331	10:42	467, 554, 656, 763, 835, 893, 953, 1042	13.9	23.5	12	12.2	98.3	22.2	6793, Smith
970417	22:09	255, 336, 410, 502, 588, 673, 763, 835, 953, 1042	12.7	24.0	30	23.6	105.9	24.1	6741, James
970517	17:09	255, 336, 410, 502, 588, 673, 763, 835, 953, 1042	10.2	25.3	43	35.4	119.2	30.1	6741, James
970518a	02:35	255, 336, 410, 502, 588, 673, 763, 835, 953, 1042	10.1	25.3	178	35.4	119.7	30.4	6741, James
970518b	09:02	255, 336, 410, 502, 588, 673, 763, 835, 953, 1042	10.1	25.3	273	35.4	119.7	30.4	6741, James
970604	01:09	255, 336, 410, 467, 502, 547, 588, 673, 835, 953, 1042	9.1	25.8	357	38.4	126.3	33.7	6793, Smith
970627a	13:50	255, 336, 410, 502, 588, 673, 763, 835, 953, 1042	7.6	26.0	323	40.5	139.4	40.3	6741, James
970627b	17:04	255, 336, 410, 502, 588, 673, 763, 835, 953, 1042	7.6	26.0	9	40.5	139.4	40.3	6741, James
970627c	20:19	255, 336, 410, 502, 588, 673, 763, 835, 953, 1042	7.6	26.0	56	40.5	139.4	40.3	6741, James

TABLE 1. *Continued*

UT Date ^a YYMMDD	Time ^b UT	Wavelengths, nm	Diameter, arcsec	SE Lat, deg	SE Lon, deg	Phase, deg	L_s , deg	Resolution, ^c km/pixel	PROGID ^d
<i>HST Cycle 7 data: WFPC2 and NICMOS</i>									
970709	00:19	255, 336, 410, 502, 588, 673, 763, 835, 953, 1042	7.1	25.5	6	40.5	145.4	43.2	7276, James
970710	00:34	255, 336, 410, 502, 588, 673, 763, 835, 953, 1042	7.1	25.4	0	40.5	145.9	43.2	7276, James
970711	02:21	255, 336, 410, 502, 588, 673, 763, 835, 953, 1042	7.0	25.4	17	40.5	146.4	43.8	7276, James
970715	03:00	255, 336, 410, 502, 588, 673, 763, 835, 953, 1042	7.0	25.3	349	40.5	146.9	43.8	6793, Smith
970723	11:30	NICMOS: 950, 970, 1080, 1130, 1450, 1660, 1900, 2120, 2150, 2160, 2370	6.9	25.1	34	40.4	148.4	44.4	7276, James
970729a	13:55	255, 336, 410, 502, 588, 673, 763, 835, 953, 1042	6.5	24.0	12	40.0	154.6	47.1	6793, Smith
970729b	17:06	255, 336, 410, 502, 588, 673, 763, 835, 953, 1042	6.5	24.0	59	40.0	154.6	43.8	6793, Smith
970729c	20:20	255, 336, 410, 502, 588, 673, 763, 835, 953, 1042	6.5	24.0	106	40.0	154.6	43.8	6793, Smith
970812	02:28	255, 336, 410, 502, 588, 673, 763, 835, 953, 1042	6.4	23.5	67	39.7	156.7	47.9	7276, James
970829	12:39	255, 336, 410, 502, 588, 673, 763, 835, 953, 1042	6.0	21.1	50	38.5	165.2	51.1	7276, James
970901	14:52	255, 336, 410, 502, 588, 673, 763, 835, 953, 1042	5.7	18.2	53	37.2	173.4	53.8	7276, James
970912	16:40	410, 502, 673, 1042	5.5	15.4	332	36.0	179.9	55.8	7792, DD
970918	02:10	255, 336, 410, 502, 588, 673, 763, 835, 953, 1042	5.4	14.0	62	35.4	182.9	56.8	7276, James
970923	01:04	410, 502, 673, 1042	5.3	12.7	359	34.9	185.8	57.9	7792, DD
970930	08:59	255, 336, 410, 502, 588, 673, 763, 835, 953, 1042	5.2	10.6	46	34.0	190.0	59.0	7276, James
971001a	01:08	255, 336, 410, 502, 588, 673, 763, 835, 953, 1042	5.2	10.4	282	33.9	190.4	59.0	7276, James
971001b	17:15	255, 336, 410, 502, 588, 673, 763, 835, 953, 1042	5.2	10.4	157	33.9	190.4	59.0	7276, James
971005	00:18	410, 502, 673, 1042	5.2	9.2	233	33.4	192.7	59.0	7792, DD
971009	01:07	410, 502, 673, 1042	5.1	8.0	203	32.9	195.1	60.2	7792, DD
<i>HST Cycle 8 data: WFPC2</i>									
990427	17:55	255, 336, 410, 502, 547, 588, 631, 673, 763, 835, 953, 1042	16.2	19.0	17	2.7	130.5	19.4	8152, Bell
990428	00:22	255, 336, 410, 502, 547, 588, 631, 673, 763, 835, 953, 1042	16.2	19.0	111	2.9	130.6	19.4	8152, Bell
990501	13:47	255, 336, 410, 502, 547, 588, 631, 673, 763, 835, 953, 1042	16.2	19.5	281	5.9	132.4	19.4	8152, Bell
990506	11:28	255, 336, 410, 502, 547, 588, 631, 673, 763, 835, 953, 1042	16.1	20.3	205	10.0	134.7	19.5	8152, Bell

^aRead 940823 as August 23, 1994. a, b, c, etc. indicates first, second, third, etc. set of images obtained on that day.

^bTime given as the start of the ~ 25 to 50 minute observing sequence.

^cResolution is the maximum spatial resolution at the sub-Earth point for images obtained on the PC or NIC1 chip.

^dSpace Telescope Science Institute Program Identification number and Principal Investigator, for *HST* data archive access.

^eCycles 0–3 resolution takes into account blurring of WF/PC images due to uncorrected spherical aberration in *HST* primary.

^fCycles 4–8 resolution takes into account COSTAR spherical aberration correction for WFPC2.

TABLE 1. *Continued*

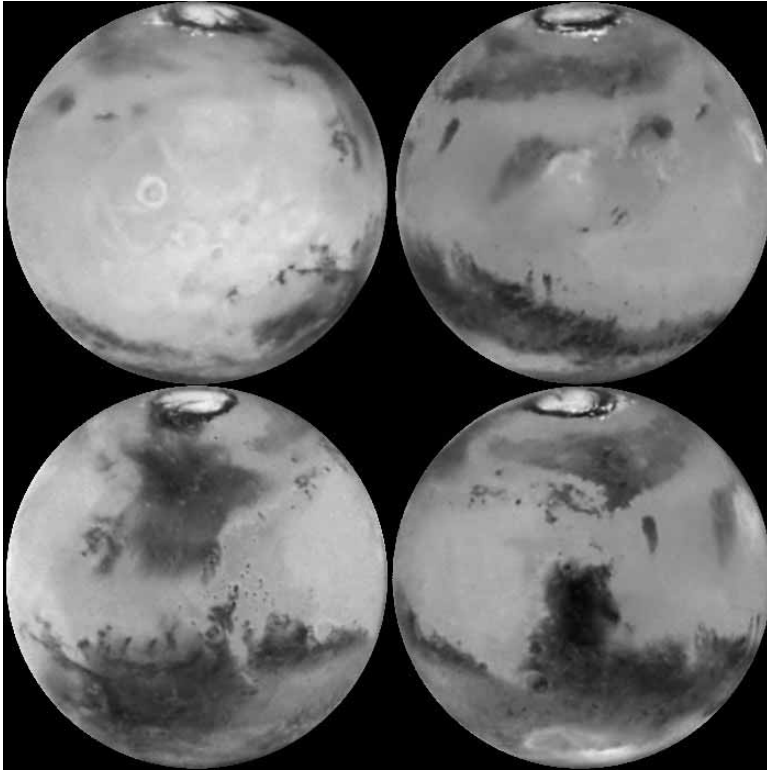


FIGURE 2.

After Cycle 4 the spherical aberration was corrected by COSTAR, and WFPC2 was able to realize the full diffraction-limited resolution of the system (Figure 2). Also, time allocation was changed to integer numbers of orbits rather than hours, meaning that additional exposures could be obtained during each visit. The important focus on blue/UV imaging was maintained, as was the seasonal sampling, but additional orbit time meant that more near-IR images could be obtained in order to characterize the surface colorimetric, mineralogic, and photometric properties. In addition to the standard filters, several of the WFPC2 linear ramp filters (LRF) were employed beginning in Cycle 5, in order to obtain photometry at key wavelengths diagnostic of broad solid state mineral absorption features.

The only NICMOS Mars observations to date were performed during a single dedicated orbit in July 1997. These observations were designed to sample the Martian near-IR reflectance spectrum at key wavelengths diagnostic of atmospheric CO_2 , CO , and H_2O as well as solid state mineral absorptions.

4.2. Spectroscopy

Table 2 summarizes *HST* spectroscopic observations during Cycles 0–8. Spectroscopy of Mars in the UV was performed using both FOS and STIS in order to characterize the composition, opacity, and spatial/temporal distribution of atmospheric aerosols. The instrument apertures were frequently positioned across both the limb and terminator in order to maximize atmospheric path length and to detect diurnal variations. FOS “pushbroom” scans and STIS slit-scans were programmed in order to obtain wider spatial coverage as well as measurements spanning specific latitudes/longitudes. STIS long-slit

UT Date YYMMDD	Time, UT	Inst. & Central Wavelength	Diam., arcsec	SE Lat, deg	SE Lon, deg	Phase, deg	L_s , deg	PROGID
<i>HST Cycle 1 data: FOS</i>								
910102	07:06	FOS, 2650 Å	13.7	-13.1	314.1	25.9	358.7	3107, James
910207	06:27	FOS, 2650 Å	9.4	-10.0	329.2	36.2	16.2	3107, James
<i>HST Cycle 2 data: FOS</i>								
920627	18:04	FOS, 2650 Å	5.8	-16.9	234.6	37.6	277.0	3763, James
920824	07:45	FOS, 2650 Å	6.8	-1.5	239.5	41.9	311.8	3763, James
<i>HST Cycle 3 data: FOS</i>								
930102	05:58	FOS, 2650 Å	15.1	8.3	71.7	5.5	20.0	4771, James
930409	14:44	FOS, 2650 Å	7.2	10.4	33.9	37.0	63.8	4771, James
<i>HST Cycle 4 data: FOS</i>								
950224	18:25	FOS, 2650 Å	13.7	17.5	294.8	10.6	63.5	5493, James
<i>HST Cycle 6 data: FOS</i>								
960918	18:40	FOS, 2650 Å	4.7	16.8	139.5	29.3	11.3	6741, James
970104	16:18	FOS, 2650 Å	8.3	23.8	144.8	35.0	60.4	6741, James
<i>HST Cycle 7 data: STIS</i>								
970708	13:28	STIS, 2375 Å	7.2	25.6	208.0	40.6	144.7	7276, James
970724	08:21	STIS, 7751 Å	6.5	24.4	338.0	40.1	152.7	7276, James
970827	10:31	STIS, 2375 Å	5.8	19.1	38.3	37.7	170.9	7276, James
971001	03:18	STIS, 2375 Å	5.4	10.4	311.1	33.9	190.4	7276, James
<i>HST Cycle 8 data: STIS</i>								
990427	19:53	STIS, 7751 Å	16.2	19.0	45.4	2.8	130.5	8152, Bell
990501	15:46	STIS, 7751 Å	16.2	19.6	310.2	6.0	132.4	8152, Bell
990506	13:26	STIS, 7751 Å	16.1	20.3	232.3	10.1	134.8	8152, Bell
990507	07:14	STIS, 7751 Å	16.1	20.4	132.7	10.7	135.1	8152, Bell

TABLE 2. *HST* FOS and STIS observations of Mars: 1990–1999
(Table heading abbreviations as in Table 1.)

spectroscopy in the visible was performed in Cycles 7 and 8 using slit scanning to build up 3-dimensional image cubes (spatial \times spatial \times spectral); due to a commanding error the scan did not work successfully in Cycle 7, but the Cycle 8 scans executed flawlessly.

5. Results

Many scientific results have been published in the peer-reviewed literature from the ~ 10 years of *HST* Mars observations. This section summarizes the major findings and discusses their implications for both science and NASA mission support. Additional details can be found in the publications cited along with each of the results discussed.

5.1. Martian atmospheric studies

5.1.1. Abundance and spatial distribution of O_3 and H_2O

Ozone and water are only trace constituents of the Martian atmosphere (0.04 to 0.2 ppm and $\sim 0.03\%$, respectively; Owen 1992), but their photolysis and recombination play critical roles in Martian atmospheric photochemistry. Specifically, the long-term stability of CO_2 against photolytic breakdown ($CO_2 + h\nu \rightarrow CO + O$) is maintained by the

breakdown and recombination of O_3 and H_2O in the Martian atmosphere (e.g. McElroy & Donahue 1972; Clancy & Nair 1996). Ozone has a photochemical lifetime of only a few hours in the Martian atmosphere, but it has been shown by Mariner 9 measurements to undergo large seasonal variations in response to changes in the Mars atmospheric water vapor profile (e.g. Barth et al. 1973). Ozone is difficult to measure on Mars from ground-based or spacecraft techniques, but *HST* can routinely provide excellent data on Mars ozone by UV spectra and imaging within the strong ~ 260 nm O_3 Hartley absorption band. James et al. (1994) used WF/PC UV imaging and an atmospheric scattering model to constrain ozone abundances and atmospheric dust and water ice cloud opacities during late northern winter ($L_s \sim 350^\circ$). Clancy et al. (1996) analyzed FOS spectral scans of Mars from Cycle 4 data (Table 2) to derive ozone column abundances and water ice cloud opacities during the Martian aphelion season. They found twice the ozone abundance as that reported from perihelion IR spectroscopy measurements (Espenak et al. 1991), consistent with photochemical and observational modeling (Clancy & Nair 1996; Clancy et al. 1996) that predicted such a seasonal middle-atmosphere ozone increase associated with lower aphelion atmospheric temperatures and lowering of the altitude of water vapor saturation (see below). This aphelion enhancement of the ozone was observed again in the next Mars year (1996–7) using FOS data (Clancy et al. 1999). *HST* observations currently provide the only way to routinely monitor the variability of ozone, and by inference water vapor, in the Martian atmosphere. As described below, *HST* observations have had a profound impact on current thinking about the stability of the Martian climate.

5.1.2. *Opacity and spatial/temporal variability of atmospheric dust and water ice clouds*

The ability to observe in the UV and to perform accurate flux calibration of *HST* imaging and spectroscopic measurements across the UV to near-IR has enabled substantial progress in the modeling of aerosol opacity in the Martian atmosphere. For example, James et al. (1994) used WF/PC images and a multiple-scattering radiative transfer model to estimate dust and water ice cloud opacities and their radiative influence on the Martian climate. They found low dust opacities ($\tau < 0.1$ – 0.2) in their December 1990 and May 1992 observations, and water ice cloud opacities near 0.2 for the winter “polar hood” clouds and typically < 0.1 for orographic or early morning limb clouds. Modeling of 1995 WFPC2 images by Wolff et al. (1997) during visibly dusty conditions (Figure 3) allowed quantitative estimates of the dust and water ice cloud opacity as well as refined values of the dust single scattering albedo. They noted the correlation between elevated dust opacities and elevated atmospheric temperatures derived from near-simultaneous microwave imaging, and postulated that the dust activity seen in the 1995 *HST* images likely followed a large regional or possibly even global dust storm which was not noticed by other groundbased observing methods. Most recently, Wolff et al. (1999) analyzed 1992–97 *HST* images to determine dust and water ice cloud opacities and to constrain further the dust single scattering albedo. Their results are consistent with near-simultaneous opacity values derived from the surface by Mars Pathfinder (Smith et al. 1997) as well as by those obtained from MGS (Clancy et al. 2000). The *HST* and MGS opacity values indicate that Mars was generally less dusty during 1992–1997 than during the same seasons during the Viking Lander missions of the late 1970s.

5.1.3. *Changes to the Viking-era climate paradigm?*

Based on a combination of groundbased microwave profiling and *HST* observations, Clancy et al. (1996) proposed a modification in the Viking-era interpretation of the Martian climate. In essence, their analysis indicated that the aphelion season on Mars

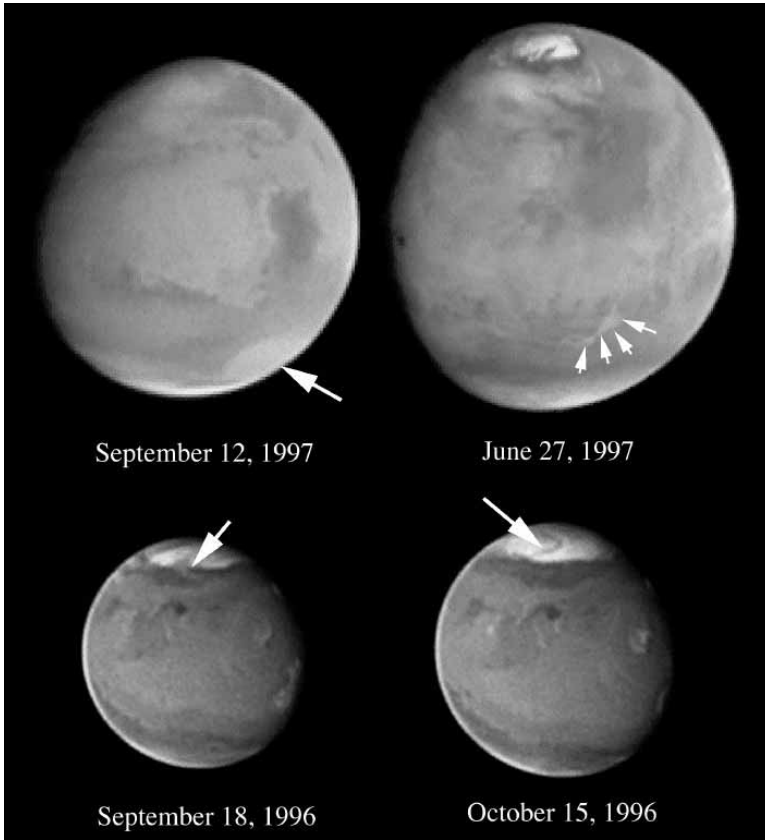


FIGURE 3.

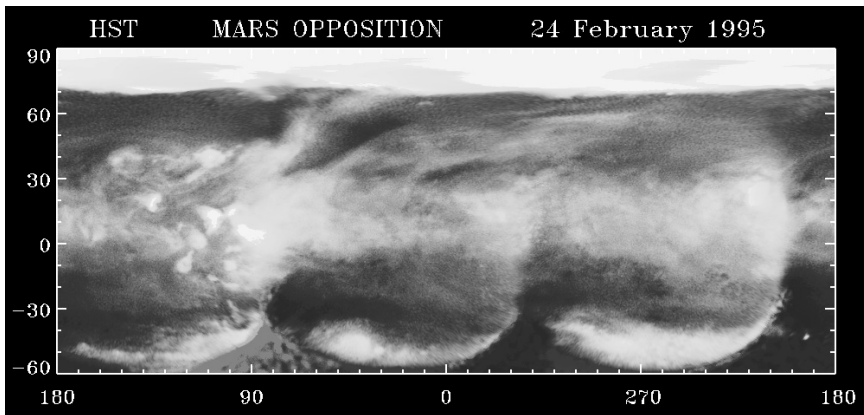


FIGURE 4.

was now colder and less dusty than during the Viking mission. Solar insolation varies by $\sim 40\%$ during the Martian year because of the planet's eccentricity, leading to 30–40 K annual variations in average atmospheric temperatures (in the absence of any other sources of radiative warming such as a large dust opacity). The lower temperatures produce a lower altitude (< 10 km) of water vapor saturation. One directly observable consequence of this different climate is that the aphelion atmosphere of Mars should

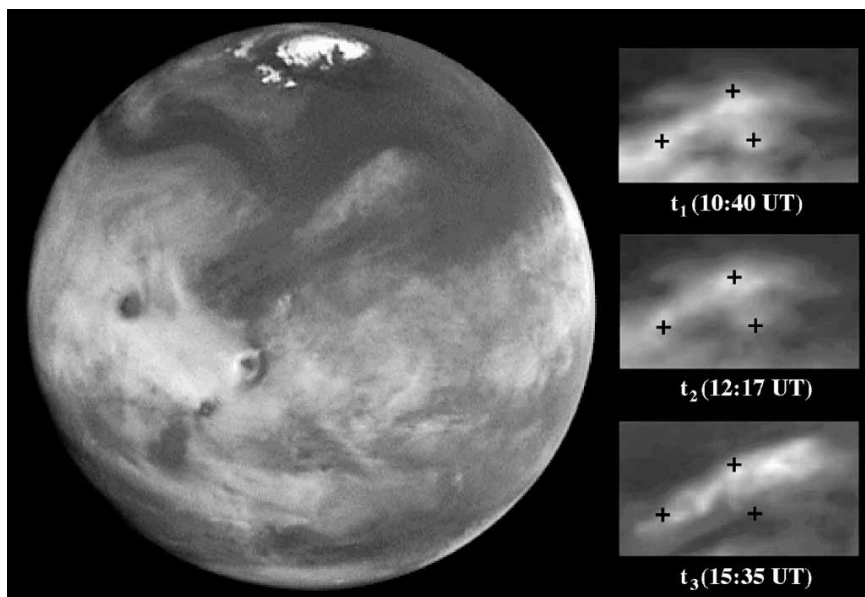


FIGURE 5.

be extremely cloudy. Until quite recently, it was thought that such cloudiness was not present during the multi-year Viking Orbiter missions of the late 1970s to early 1980s. This fact was addressed by Clancy et al. (1996) with the suggestion that the Viking-era atmosphere was much more dusty than “usual,” and that this elevated dust provided a source of radiative heating sufficient to prevent the atmosphere from transitioning to the cooler, cloudier aphelion state. Groundbased optical and IR observations of Mars near aphelion are typically of poor quality because even at opposition the planet is always far from Earth (Figure 1), and so *HST* observations in the mid-1990s provided the first opportunity to test (separately from the microwave data) this “cold and cloudy” vs. “warm and dusty” hypothesis. Figure 4 shows a composite map of 410 nm images from February 1995—an equatorial “belt” of enhanced cloudiness is apparent in these and other *HST* image near aphelion (as well as some older photographic data reported by Slipher 1962), consistent with the Clancy et al. (1996) aphelion climate. A quantitative *HST* study of water ice cloud opacity during the 1990s by Wolff et al. (1999) corroborated the presence of an extensive aphelion equatorial cloud belt for three sequential Martian years. The recent discovery of a bias in the Viking data used to derive atmospheric temperatures (previous ones are 15 to 20 K too warm) (Richardson & Wilson, 2000) and the apparent presence of the aphelion cloud phenomenon in some of the Viking observations (Tamppari et al. 2000) have further highlighted the reality of the Clancy et al. finding. Although much of the original motivation for the Clancy et al. climate model derived from microwave measurements, *HST* observations of the aphelion cloud belt provided a critical piece of evidence that could not be ignored.

5.1.4. *Atmospheric circulation*

The advent of WFPC2 observations during Cycle 4 provided the ability to obtain spectacular UV and blue images of fine-scale structure in the Martian atmosphere (Figure 5), thus allowing cloud feature tracking to derive wind speed and wind direction data and to compare them with predictions from General Circulation Models (GCMs) for specific seasons. Mischna et al. (1998) analyzed Cycle 6 WFPC2 UV/blue images and identified

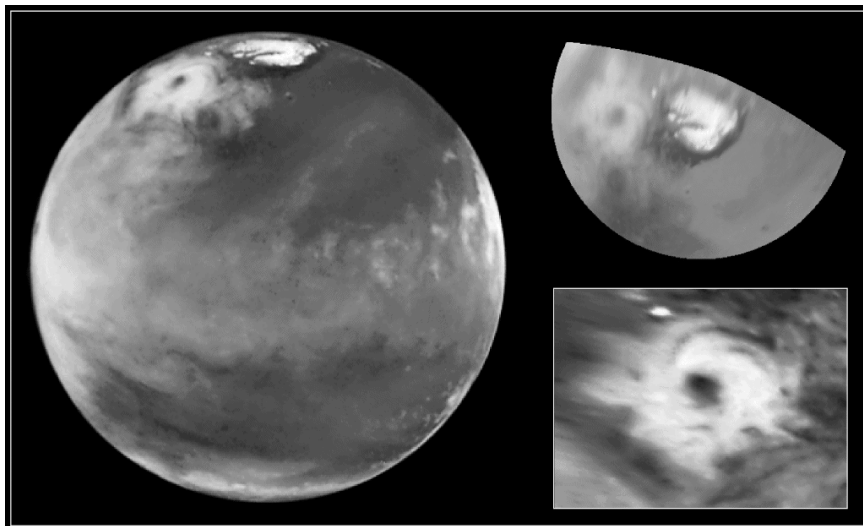


FIGURE 6.

specific cloud features that could be tracked over a 5 hour time span between images. They found average wind speeds of $\sim 30 \pm 10$ m/sec for the features studied. Both the speeds and the determined wind directions of the clouds were found to be consistent with GCM predictions for early northern summer midlatitudes (Haberle et al. 1993). More recently, Gierasch & Bell (2000) report the detection of a huge cyclonic storm system in Cycle 8 WFPC2 imaging during northern summer (Figure 6). This spiral storm is similar in form to those seen during summer at high northern latitudes by the Viking Orbiter mission (Gierasch et al. 1979) except that it was much larger. Groundbased amateur observers (M. Minami, pers. comm., 1999) report possible evidence for the existence of the storm at least several days before the *HST* observations, but additional *HST* imaging just 6 hours after the discovery observations show it to have rapidly dissipated. MGS Mars Orbiter Camera (MOC) or laser altimeter observations were not obtained at the same time as the *HST* data, but MOC data taken a few days later show evidence for similar short-lived spiral structures in the north polar region (M. Malin, pers. comm., 1999). The *HST*, MOC, and Viking data combined indicate that spiral water ice storms are a common feature of the northern summer polar latitudes. Gierasch and Bell (2000) postulate that these systems may be fueled by the strong temperature gradient between the cold polar atmosphere and the warmer surface of the dark circumpolar sand dunes, much like “polar low” storms on the Earth are fueled by oceanic temperature gradients.

5.2. *Martian surface studies*

5.2.1. *Oxidation state of Fe in the surface materials*

Groundbased telescopic observations of Mars at visible wavelengths have previously revealed that the surface has a steep red spectral slope caused by the presence of oxidized surface minerals with Fe(III) solid state absorptions in the blue to UV (e.g. Adams & McCord 1969; Singer et al. 1979; Bell et al. 1990). Evidence for Fe(II) absorption features caused by relatively unoxidized surface materials, primarily in low albedo regions, has also been presented in these same studies from measurements in the near-infrared, especially near $1.0 \mu\text{m}$. The region near $1.0 \mu\text{m}$ includes absorption from both Fe(II) and Fe(III) solid state mineral features, however, and so inferences regarding the oxidation state of low albedo regions of Mars must properly separate the effects of both ferric and ferrous

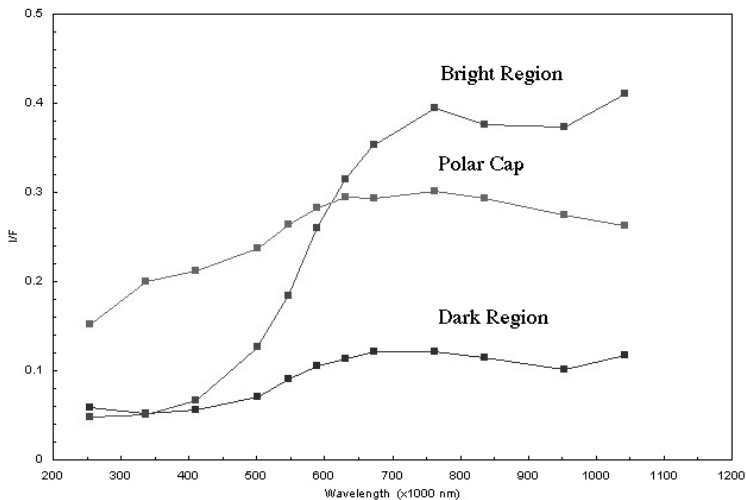


FIGURE 7.

mineral bands in the near-IR (e.g. Morris et al. 1995). Such unmixing is confounded in groundbased studies by the presence of strong telluric absorption near $0.95 \mu\text{m}$ which can hamper or destroy the ability to properly model the spectral reflectance across the $1 \mu\text{m}$ band. *HST* measurements are free of telluric contamination and thus provide the ability to properly measure and model this important spectral region. Examples of WFPC2 spectra assembled from multiple narrowband images are shown in Figure 7 (Bell et al. 1999). These data, combined with *HST* multispectral imaging from earlier Cycles (James et al. 1996; Bell et al. 1997), has confirmed that most low albedo, classical “dark” regions of Mars contain a substantial Fe(II) component diagnostic of relatively unweathered and unoxidized volcanic material like pyroxene, mixed with and/or partially covered by small amounts of a much more heavily oxidized Fe(III) component diagnostic of poorly crystalline or nanophase iron oxide. However, the *HST* studies also reveal the existence of anomalous dark regions that appear dominated by ferric rather than ferrous minerals, and may represent the discovery of a new class of surface materials with spectral properties consistent with *hydrated* ferric oxides like goethite ($\alpha\text{-FeOOH}$) or ferrihydrite ($\sim 5 \text{Fe}_2\text{O}_3 \cdot 9\text{H}_2\text{O}$) rather than anhydrous ferric oxides like hematite ($\alpha\text{-Fe}_2\text{O}_3$) (Bell, 1992; Murchie et al. 1993, 2000; Bell & Morris 2000). If confirmed by additional telescopic and spacecraft investigations, this discovery may indicate regions on Mars where liquid water was extensively involved in the weathering and alteration of surface materials. While OH- or H_2O -bearing minerals should be unstable and should dehydroxylate under present Martian climatic conditions (very low $p(\text{H}_2\text{O})$, high UV flux), they could exist metastably because of extremely low temperatures and/or burial within a mixed regolith (e.g. Burns, 1993, Yen et al. 1999).

5.2.2. *Global-scale spectral unit mapping*

The multispectral properties of surface materials on Mars provide diagnostic information on their composition and physical nature. During the Viking Orbiter investigation in the mid 1970s, imaging observations as the spacecraft approached Mars were used to discriminate distinct surface units based on their 3-color (blue, green, red) spectral properties (Soderblom et al. 1978; McCord et al. 1982). Differences in color were related to potential differences in mineralogy, oxidation state, particle size, and/or degree of surface

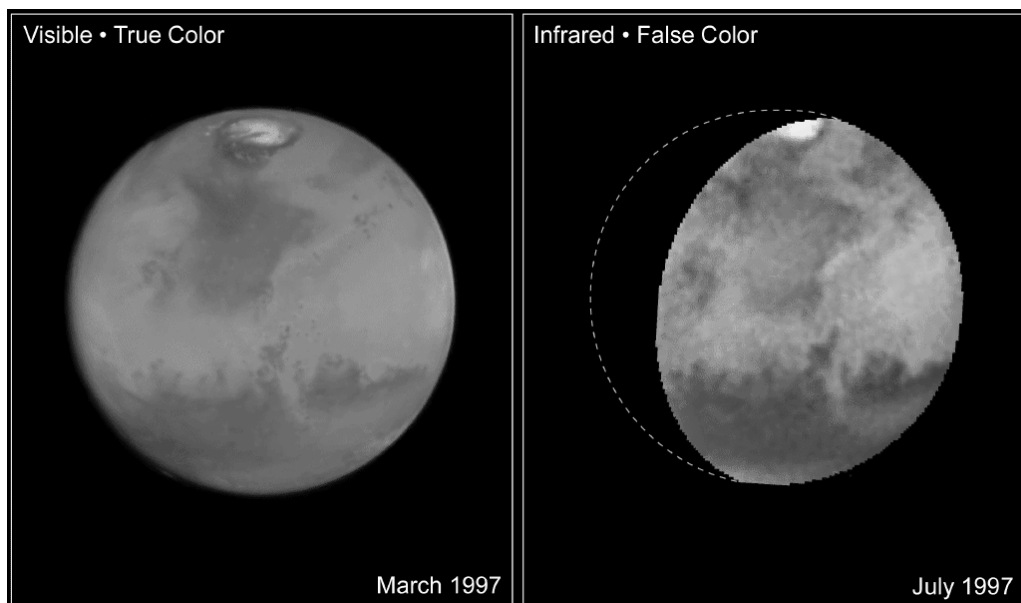


FIGURE 8.

compaction (fine dust vs. cemented duricrust). *HST* provides unique new data that can extend the Viking-era spectral unit study to higher latitudes and longer wavelengths at a comparable spatial scale (tens of km/pixel). Initial analyses of eastern hemisphere spectral units by Bell et al. (1997) showed broad consistency with the Viking-derived spectral units, but was augmented by the ability to discriminate further by using WFPC2's near-IR filters to reveal additional reflectance trends not identifiable in previous (or current) spacecraft datasets.

5.2.3. *Unique surface mineralogic deposits*

The combination of WFPC2 and NICMOS imaging observations of Mars provides the ability to cover broad regions of the solar reflectance spectrum at spatial scales unobtainable from groundbased telescopes and in spectral regions not being measured by spacecraft, and thus to identify unique spectroscopic signatures from surface materials. Two examples have been reported from preliminary analyses of Cycle 7 and 9 Mars images. First, NICMOS observations during Cycle 7 provided evidence for the presence of spatial variations in the distribution of H₂O- or OH-bearing minerals on the surface (Bell et al. 1998). The Martian surface has long been known to contain a small amount (1 to 3%) of such hydrated minerals, although their specific mineralogic identity has not been determined (e.g. Houck et al. 1973; Pimentel et al. 1974). The NICMOS data, showing variations in the strength of an H₂O vibrational overtone absorption near 1450 nm (Figure 8), have not revealed the identity of the hydrated mineral(s) on the surface, but they have revealed spatial variations in the abundance and/or composition of the hydrated material, especially within the classical dark regions. Continuing analyses are searching for correlations between these variations and other geologic or spectroscopic properties of the surface, in the hopes of identifying the specific mineralogy. Second, WFPC2 Cycle 6 observations in the near-IR revealed the presence of extremely strong absorption near 953 nm isolated to a dark ring of material surrounding the north polar cap (Bell et al. 1996, 1997; Figure 9). This dark material is known to include large expanses of sand dunes and other aeolian features based on Viking Orbiter imaging. The *HST* data have been

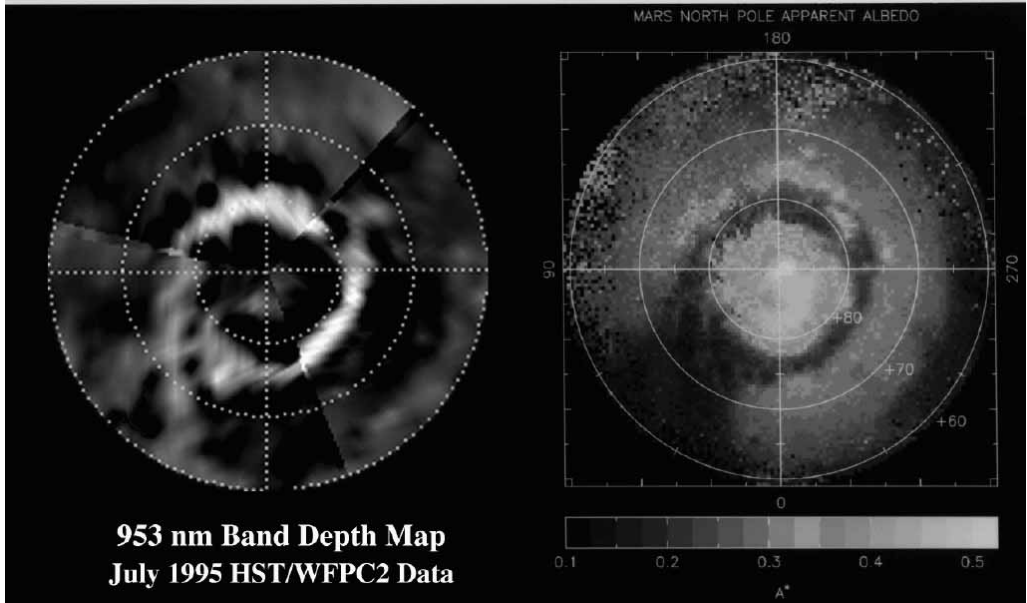


FIGURE 9.

interpreted to indicate the presence of extremely “fresh” or unoxidized deposits of the igneous mineral pyroxene. The pyroxene signature in the north polar sand sea appears broadly similar to that observed from groundbased telescopes and *HST* in other dark regions of the planet (e.g. Singer et al. 1979; Bell et al. 1997), but this geologic region has either a higher pyroxene abundance, a larger pyroxene grain size, and/or a different composition that leads to a stronger band depth. One proposed model accounts for the stronger bands through a comet-like “sublimation gardening” effect, whereby grains are continually being jostled and freed of dust coatings by the diurnal and seasonal exchange of CO_2 between the polar surface and atmosphere (Bell et al. 1997). This and other models are being tested and refined using higher resolution and extended wavelength coverage of the same region of the planet obtained by WFPC2 during Cycle 8 (Bell et al. 2000).

5.2.4. *Surface albedo changes on seasonal and interannual timescales*

Mars has exhibited changes in surface albedo markings throughout the history of telescopic observations. These variations in albedo markings are caused by aeolian deposition or removal of bright, red, heavily oxidized dust over regions of intrinsically lower albedo. When seasonal or interannual wind circulation patterns change, dust that was preferentially deposited after local or global-scale dust storms can be swept clean, exposing a darker surface. Telescopic and spacecraft observations have shown that the dust particles are only a few microns in size on average (e.g. Pollack et al. 195; Ockert-Bell et al. 1997), and thus they are easily transportable by winds of a few tens of meters per second in the thin Martian atmosphere. Laboratory studies have shown that only a few tens of microns or less of dust are required to optically brighten a low albedo surface (Wells et al. 1984; Johnson et al. 2000). Therefore, changes in the surface albedo distribution can be used to identify changes in global atmospheric circulation patterns, and serve as a proxy for understanding the variability of the current Martian climate. *HST* has provided new insight in this area by revealing surface albedo changes over a ~ 10 year period and at an unprecedented spatial scale. The most prominent reported change is the

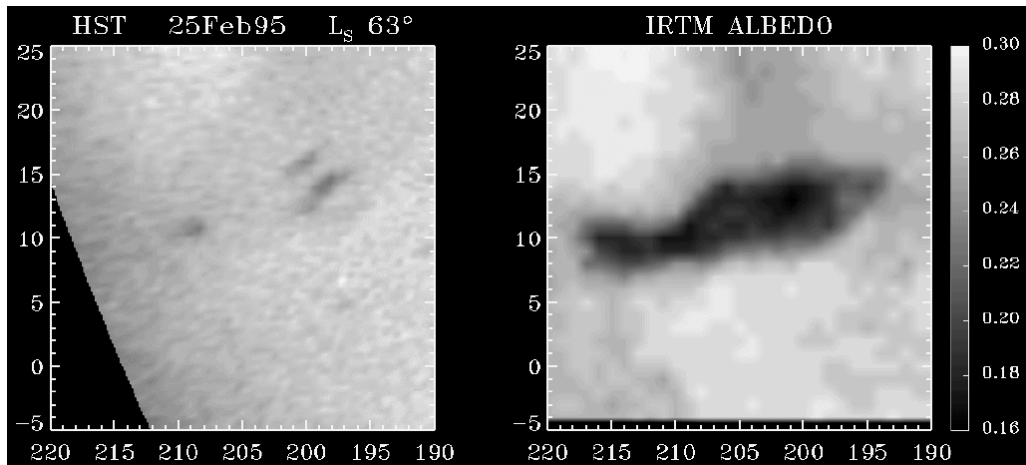


FIGURE 10.

near-complete disappearance of a California-sized low albedo region called Cerberus in the planet's eastern hemisphere (Lee et al. 1996), between the end of the Viking mission in the early 1980s and *HST* observations in the 1990s (Figure 10). Apparently, changing atmospheric circulation patterns during this time resulted in the preferential deposition of windblown dust on top of this feature. Groundbased thermal IR observations of this part of the surface, combined with the *HST* observations, indicate a layer of dust perhaps as thick as 1–2 mm deposited onto the surface over a 5 to 10 year period (Moersch, 1998). The implied dust deposition rate ($\sim 400 \mu\text{m}/\text{yr}$) is at the very high end of that inferred from other types of observations, and may indicate the presence of substantial regional or global-scale dust storm activity during the post-Viking but pre-*HST* period.

5.2.5. Growth and recession of the polar caps

The most obvious and measurable manifestation of the changing Martian seasons is the waxing and waning of the planet's seasonal polar ice caps. Each fall and winter, nearly 25% of the atmospheric mass condenses out at the poles to form meters-thick deposits of CO_2 frost. Each spring and summer, the CO_2 sublimates back into the atmosphere, exposing in the north a residual water ice polar cap, and in the south either bare surface some years or a small $\text{H}_2\text{O}+\text{CO}_2$ residual ice cap. Variations in the growth and decay rates of the seasonal polar caps have been observed for centuries telescopically, and these variations reveal short-term fluctuations in the current Martian climate (James et al. 1992). *HST* provides the ability to monitor polar cap recession at scales comparable to previous Mariner 9 and Viking Orbiter imaging, and thus to make detailed comparisons of year-to-year climate variability based on small-scale feature variations. Both James et al. (1996) and Cantor et al. (1998) have analyzed *HST* images of Mars polar cap retreats during the 1990s and have found evidence for differences between the behavior of the cap in the 1990s and that reported from previous epochs. The source of the changes is thought to be related to variations in annual dust storm variability, which can substantially change the seasonal variation of the diurnal atmospheric temperature profile.

5.2.6. High resolution imaging spectroscopy

Most recently, *HST* and STIS have been used to obtain imaging spectroscopic data of Mars in the visible to near-IR and at high spatial and spectral resolution (Bell et al.